LOCAL OSCILLATOR INDUCED DEGRADATION OF MEDIUM-TERM STABILITY IN PASSIVE ATOMIC FREQUENCY STANDARDS*

G. J. Dick, J. D. Prestage, C. A. Greenhall, and L. Maleki

California Institute of Technology
Jet Propulsion Laboratory
4800 Oak Grove Drive
Pasadena, California 91109

Abstract

As the performance of passive atomic frequency standards improves, a new limitation is encountered due to frequency fluctuations in an ancillary local oscillator (L.O.). The effect is due to time variation in the gain of the feedback which compensates L.O. frequency fluctuations. The high performance promised by new microwave and optical trapped ion standards may be severely compromised by this effect.

We present an analysis of this performance limitation for the case of sequentially interrogated standards. The time dependence of the sensitivity of the interrogation process to L.O. frequency fluctuations is evaluated for single-pulse and double-pulse "Ramsey" RF interrogation and also for amplitude modulated pulses. The effect of these various time dependencies on performance of the standard is calculated for an L.O. with frequency fluctuations showing a typical $1/f$ spectral density. A limiting $1/\sqrt{\tau}$ dependent deviation of frequency fluctuations is calculated as a function of pulse lengths, dead time, and pulse overlap.

We also present conceptual and hardware-oriented solutions to this problem which achieve a much more nearly constant sensitivity to L.O. fluctuations. Solutions involve: use of double-pulse interrogation; alternate interrogation of multiple traps so that the "dead time" of one trap can be covered by operation of the other; and the use of double-pulse interrogation for two traps, so that during the time of the RF pulses, the increasing sensitivity of one trap tends to compensate for the decreasing sensitivity of the other. A solution making use of amplitude-modulated pulses is also presented which shows nominally zero time variation.

INTRODUCTION

As the performance of passive atomic frequency standards improves, a new limitation is encountered due to frequency fluctuations in the local oscillator (L.O.) from which RF interrogation signals are derived[1-3]. This limitation continues to the longest times, giving frequency deviations which show the same $1/\sqrt{\tau}$ dependence on measuring time τ as the inherent performance of the standard itself. It is due to periodic time variation of the gain in the feedback which keeps the L.O. frequency locked

*This work was carried out at the Jet Propulsion Laboratory, California Institute of Technology, under a contract with the National Aeronautics and Space Administration.

to the atomic line. The varying gain aliases higher frequency L.O. fluctuations to frequencies near zero frequency, and these low frequency detected signals are improperly compensated by the feedback process.

Practical atomic interrogation processes show a sensitivity to L.O. frequency which is not constant with time. This arises because e.g. the high and low frequency sides of the atomic absorption line are alternately interrogated to compensate for signal strength variability. Furthermore, a "dead time" with consequent zero sensitivity is characteristic of newly developed standards using sequential interrogation. These include both microwave and optical frequency versions of the trapped ion standard. The higher performance promised by these new standards is severely compromised by presently available L.O. capability.

In the following sections we examine the time dependence of the sensitivity to L.O. frequency which is inherent in single- and double pulse (Ramsey) sequential RF interrogation processes. Details of the electromagnetic transition are calculated using a conventional spin flip analogue. This treatment allows the effect of time-varying phase or amplitude of the exciting RF signal to be calculated by means of appropriate solid-body rotations of an initial state vector.

We propose the use of several alternately-interrogated collections of atoms or ions (several "traps") to allow a net sensitivity which is much more nearly constant in time. Detailed strategies are developed, including one which uses amplitude modulated RF pulses with a particular form which can give a net sensitivity for the two traps which shows nominally zero time variation.

The effect of any given time varying sensitivity on performance of the atomic standard depends on the spectrum of frequency fluctuations for the L.O. We present the results of numerical and analytical calculations for the effect of an L.O. with flicker frequency noise and consequent flat Allan deviation as a function of measuring time τ.

Finally, block diagrams are shown for implementations of a trapped mercury ion frequency standard with two ion collections, including one with two ion collections in a single linear trapping structure. Various systematics are addressed, including sensitivities to signal strengths and RF phase shift values.

BACKGROUND

Passive atomic and ionic frequency standards presently provide greater long term stability than any other frequency sources. They include the new Trapped Mercury Ion standards[1-6], more conventional Rubidium[7] and Cesium standards[8,9], and the optical standards[10] which are proposed for even higher stability. These standards have an inherent advantage for long term stability which derives from the energy gain which is available from atomic transitions which can be linked in a causal way. Thus, a low energy microwave photon may be absorbed in an ultra stable atomic transition process that then makes possible the scattering of optical photons with energy increased by more than 10^4. This makes possible a tremendous increase in sensitivity and allows passive standards to operate with very small numbers of atoms or ions. By the use of electromagnetic traps, these few atoms or ions can be isolated from each other and from their environment much more effectively than can the many atoms or ions required by active standards. This isolation reduces the effects of time varying external variables on the operating frequency, and allows the frequency of the standard to more closely approximate the inherent unvarying atomic transition frequency of a single isolated atom or ion.

However, by the nature of this process, passive frequency sources do not themselves emit a signal at

their operational frequency as do active sources. Instead, they require a secondary frequency source to interrogate the very narrow absorption line in the isolated atoms or ions. This interrogation process necessarily takes a certain amount of time, during which time the secondary local oscillator (L.O.) acts alone to provide frequency stability. Information obtained in the interrogation processes is then used to adjust the frequency of the L.O. by feedback and to stabilize it over long periods of time with great precision.

The consequence of this is most easily understood with respect to a portion of the interrogation cycle called "dead time". During this time the local oscillator's frequency is not sensed by the atomic interrogation process and so local oscillator frequency fluctuations during those times are not corrected by the feedback process. The cumulative effect of oscillator phase wander during the dead time for each cycle reduces the long term stability obtainable with the atomic standard. If the dead time could be reduced to zero, the long-term instability induced by the L.O. could also be reduced.

The dead time cannot be eliminated, however, because interrogation of the atoms or ions necessarily involves processes which degrade the Q and shift the frequency of the atomic line. The strategy which allows the highest ultimate stability is to perform these processes during dead times to minimize their interference with operation of the standard. The processes include; illumination with an intense optical beam which prepares the quantum state of the atoms or ions and which induces light scattering, the intensity of which is analyzed to determine frequency errors in the local oscillator and to correct them; adding more ions to the trap to make up for those that have been lost; and other similar processes such as vibrating the ion cloud to measure the number of ions in order to hold the number very nearly constant in time.

TIME DEPENDENCE OF FREQUENCY SENSITIVITY

Definition of a Time–Dependent Frequency Sensitivity

The lineshape, bandwidth, and resolving power for an atomic transition induced by means of electromagnetic (RF) pulses are well known[11]. Of importance to frequency standard applications is the frequency resolving power which can be written in terms of a dimensionless frequency sensitivity parameter g as

$$\frac{dp}{d\nu} = \pi g t_i, \tag{1}$$

where p is the probability for the transition, t_i is the time for the RF interrogation process, and ν is the applied RF frequency. For the case of single π-pulse interrogation and for atoms initially in the ground state, the conventional lineshape[11] gives $p = 1$ at the resonant frequency, and a resolving power described by

$$g_\pi \approx 0.60386 \tag{2}$$

at the half-bandwidth points ($p = 0.5$). Double pulse (Ramsey) interrogation using two $\pi/2$ pulses shows a narrower bandwidth and increased resolving power compared to single pulse excitation[12]. In the limit of very short excitation pulses at the beginning and end of the interrogation period, the frequency sensitivity approaches a limit of

$$g_{max} = 1. \tag{3}$$

The conventional treatment, however, does not allow a study of the effect of a frequency which varies during the excitation process. In order to accomplish this task, we generalize the frequency sensitivity

g to allow time variation during the interrogation process. If the phase fluctuations involved in the frequency variation are small ($\delta\phi << 1$), we can assume that fluctuations at all points in the process combine linearly. For this case we can generalize Eq. 1 to describe the variation in transition probability δp due a time–varying frequency error $\delta\nu(t)$ in terms of an integral over the RF interrogation time

$$\delta p = \pi \int_{RF} \delta\nu(t)\, g(t)\, dt. \tag{4}$$

Application of a non–varying $\delta\nu$ to Eq. 4 recovers Eq. 1 by relating the constant g to an integral over $g(t)$ as

$$g\, t_i = \int_{RF} g(t)\, dt. \tag{5}$$

Eq. 1 may be rewritten

$$g = 2\frac{dp}{d(\Delta\phi)} \tag{6}$$

where $\Delta\phi \equiv 2\pi\,\nu\, t_i$ is the phase progression during the course of the interrogation. In order to evaluate the time–dependent $g(t)$ for Eq. 4, let $\delta\nu(t)$ be zero except for a phase step of size ϵ at time t' given by $\phi = \epsilon\,\sigma(t - t')$, where $\sigma(x) = 1$ for $x \geq 0$ and is zero otherwise. Since $2\,\pi\,\delta\nu = d\phi/dt$, this corresponds to a frequency variation $\delta\nu(t) = (\epsilon/2\pi)\delta(t - t')$, where $\delta(t - t')$ is the Kronecker delta function. Eq. 4 gives the response

$$\delta p(t', \epsilon) = \pi \int_{RF} \frac{\epsilon}{2\pi}\delta(t - t')\, g(t)\, dt \tag{7}$$

$$= \frac{\epsilon}{2} g(t'), \tag{8}$$

so that $g(t')$ can be written in terms of the effect of a small phase step at time t'

$$g(t') = 2\frac{\delta p(t', \epsilon)}{\epsilon}. \tag{9}$$

That is, $g(t)$ describes the sensitivity of the final atomic state to a small phase step in the interrogating field at the time t. This dependence may be calculated directly by means of a detailed look at the quantum–mechanical transition process.

Analysis of L.O. Phase Step in Rotating System

The processes which determine the rate of excitation of atoms or ions from one energy state to another are explicitly quantum–mechanical. Following Kusch and Hughes[11] we find the time dependence of the phase and amplitude for the excited state by a magnetic spin–flip analogue. For the case where the two–level system consists of a particle with spin 1/2 in a magnetic field, there exists a one–to–one correspondence between the expectation values of quantum–mechanical picture and the classical picture of a magnetic moment precessing in its applied field. Only the absolute phase, a physically meaningless quantity, is missing from the classical picture. Since all weakly–coupled two–level quantum mechanical systems may be treated with identical formalism, the magnetic–moment precession analogue is generally applicable to calculate the details of transition amplitudes and phase in quantum–mechanical two level systems.

In this analogue as depicted in Fig. 1a), a vertical magnetic field $H_o = \omega_o/\gamma$ generates an energy difference between "down" and "up" states of a moment with magnitude γ and direction I. A transverse microwave field H_1 at frequency ω_{rf} is approximately tuned to the precession rate of the moment in the presence of the field H_o. Transformation to a reference frame rotating at ω_{rf} removes the rapid time variation due to spin precession in the large field H_o, leaving only a slow precession in the rotating frame. The transition problem can thus be treated entirely by the use of solid-body rotations.

In this context, detuning of the microwave frequency results in incomplete cancellation of the vertical dc field. The remaining, uncompensated, part of the vertical field combines with the transverse rf field H_1 to give an effective field in the rotating frame H_{eff}. The time dependent solutions are (slow) precessions of the magnetic moment I about this effective field at an angular rate ω_{eff} which is proportional to the magnitude of that field. Phase deviations due to the L.O. give rise to rotations about the z-axis.

All starting vectors lie in the plane, including the starting position of the unit vector $I_{initial}$, a fact which makes the algebraic relationships between the various frequencies apparent. The quantum-mechanical correspondence for the precession of I about ω_{eff}, identifies a correspondence between the vertical component of a unit vector $\hat{I}_{final}$ with the transition probability; more specifically, it is equal to the fractional occupation difference between upper and lower states at the end of the transition.

Figure 1b) shows the precession of I for the case of a π pulse on resonance. Figure 2 shows a three dimensional view of the effect of this same pulse when detuned to the half-signal point. Vertical lines are drawn from $z = 0$ plane to the arc which describes the time evolution of the atomic state. This arc is traversed by I at a uniform angular velocity during the interrogation process.

Figures 3 and 4 describe the processes used to calculate $g(t)$ for single π pulse excitation via Eq. 9. Here, I precesses about H_{eff} for a fraction of the interrogation process (until time t), a small phase step is introduced in the RF field (rotation about the z axis), and then the precession about H_{eff} is completed. The phase steps give rise to variation in the z component of the I_{final} which depends on where the step takes place; and this dependence defines $g(t)$.

Solutions

Details of the calculations for $g(t)$ based on the rotation transformations just described have been previously presented[1]. Figure 5 shows the results for three different interrogation processes. The cycle time t_c, interrogation time t_i, and dead time t_d are identified.

The functional form for the sensitivity $g(t)$ for the case of a single π-pulse at the half-bandwidth point as indicated in Figs. 2, 3, and 4 and as shown in Fig. 5a) is given by

$$g(t) = \frac{\Delta}{(1+\Delta^2)^{3/2}} \left[\sin(\Omega_1(t))\,(1-\cos(\Omega_2(t)) + \sin(\Omega_2(t))\,(1-\cos(\Omega_1(t))\right] \tag{10}$$

$$\begin{aligned} \text{where} \quad \Omega_1(t) &= \Omega \cdot \left(\frac{t}{t_i}\right), \\ \Omega_2(t) &= \Omega \cdot \left(1 - \left(\frac{t}{t_i}\right)\right), \end{aligned} \tag{11}$$

$$\Omega = \Omega(\Delta) = \pi\sqrt{1+\Delta^2}, \tag{12}$$

and where $\Delta \equiv 2\,\delta\nu\,t_i$ is detuned to the half signal point $\Delta = \Delta_{half} \approx 0.798685$. For this case the

angle of H_{eff} from the z axis (Figure 1a)) is given by

$$\theta = \theta(\Delta) = \pi/2 + \arctan \Delta. \tag{13}$$

It is worthy of note that integration of $g(t)$ as given by Eq. 10 returns the value given by Eq. 2 for this same interrogation process, i.e.

$$\int_0^{t_i} g(t)\, dt = 0.60386\, t_i. \tag{14}$$

The case of double $\pi/2$-pulse RF excitation at the resonant frequency and with a $\pi/2$ phase shift between pulses gives maximum sensitivity of the resulting measurement to frequency deviations of the L.O., and shows a particularly simple form for the time dependence of the sensitivity. As shown in Fig. 5b) its form is given by

$$\begin{aligned} g(t) &= \sin(\pi t/2t_p) && 0 < t < t_p, \\ &= 1 && t_p < t < t_i - t_p, \\ &= \sin(\pi \tfrac{t_i - t}{2t_p}) && t_i - t_p < t < t_i, \end{aligned} \tag{15}$$

where t_p is the short pulse time, and t_i the interrogation time as before.

Figure 5c) shows the time dependence for double-pulse interrogation with very narrow RF pulses to be essentially constant except for the dead time.

Use of Two Traps for More Nearly Constant Sensitivity

While a substantial "dead time" is required for a single trap, use of several, separately interrogated, sets of atoms or ions (several traps) would allow interrogation of one trap during the other's dead time. In this way the interrogation process could be almost seamless, thus apparently approaching the goal of continuous interrogation. Two traps are usually sufficient since a duty factor of $\Delta_d > \approx 50\%$ can be obtained for each trap. If it cannot, more traps could be used.

The duty cycles shown in Figure 5 point the way to interrogation strategies for two traps. Single pulse interrogation as shown in 5a) shows large variability, even without the effect of dead time. In contrast, the two pulse example shown in 5c) represents some kind of ideal. Here the infinitesimally short RF pulses give an unvarying sensitivity except for the dead time. However, RF pulse lengths cannot be shortened arbitrarily due to the increasing RF power required and the necessity to average out effects of the thermal motion of the atoms or ions[4]. Thus Fig. 5b), with functional form as given in Eq. 15 and with explicit consideration of turn on and turn off effects for double pulse interrogation allows us to examine the effects of RF pulse length and of various strategies of pulse timing. It seems clear that the starting pulse for one trap should more or less coincide with the ending pulse for the other.

Figure 6 shows the sensitivity variation for several interrogation strategies using two traps. Parts b), c), and d) show examples of the way double pulse interrogation could be used. A comparison of parts b) and c) shows that overlapping the pulses for the two traps gives a somewhat more constant sensitivity. In addition, we can calculate an optimum overlap by equating the areas above and below the line given by $g(t) = 1$. This condition minimizes the effect of the lowest frequency L.O. fluctuations and results in a sequence where the starting pulse for one trap begins slightly later than the ending pulse for the other, for a total combined pulse time $4/\pi$ times longer than a single pulse. Fig. 6d) shows that the deviation of the sensitivity from unity has been substantially reduced.

A strategy using amplitude modulated RF pulses

As a final enhancement, the use of amplitude-modulated pulses with particular shapes would allow a sensitivity with no deviation from unity, even during the time of the overlapping pulses. The requirement is, of course, that the two sensitivities not vary. One approach is to have the pulses overlap completely, and to adjust the RF amplitudes in the two traps $A_1(t)$ and $A_2(t)$ so that the sensitivities for the two traps obey

$$g_1(t) + g_2(t) = 1 \tag{16}$$

during the time of the overlap. During other times one trap would have the constant sensitivity required while the other would experiencing its dead time. Without derivation, we present the results of a generalization of the calculation in [1] which gave rise to Eq. 15. This more general calculation shows that Eq. 15 can be rewritten for amplitude-modulated RF pulses over the time interval $0 \leq t \leq t_p$ as;

$$g_1(t) = \sin\left(\frac{\pi}{2\,t_p}\int_0^t A_1(t)\,dt\right) \tag{17}$$

for the trap which is just beginning its interrogation, and

$$g_2(t) = \cos\left(\frac{\pi}{2\,t_p}\int_0^t A_2(t)\,dt\right) \tag{18}$$

for the second trap which is ending its interrogation and which will now begin housekeeping tasks. Here, $A_1(t) = A_2(t) = 1$ recovers the solutions given by Eq. 15. Solutions of Eqs. 17 and 18 which also satisfy Eq. 16 are not unique. However, analytical solutions can be found for a particularly symmetric form for the two contributions which satisfy Eq. 16 and which have the sine-squared and cosine-squared dependencies

$$g_1(t) = \sin^2\left(\frac{\pi t}{2\,t_p}\right) = \frac{1}{2}\left[1 - \cos\left(\frac{\pi t}{t_p}\right)\right] \tag{19}$$

for the starting pulse of trap 1 and

$$g_2(t) = \cos^2\left(\frac{\pi t}{2\,t_p}\right) = \frac{1}{2}\left[1 + \cos\left(\frac{\pi t}{t_p}\right)\right] \tag{20}$$

for the ending pulse of trap 2 for times $0 \leq t \leq t_p$. Solution of the integral equations 17 and 18 for these examples yields

$$A_1(t) = \frac{2}{\sqrt{1 \div \left(\sin\frac{\pi t}{2\,t_p}\right)^{-2}}} \tag{21}$$

for the beginning pulse and

$$A_2(t) = \frac{2}{\sqrt{1 + \left(\cos\frac{\pi t}{2\,t_p}\right)^{-2}}} \tag{22}$$

for the ending pulse.

Details of pulse timing for this example of amplitude modulated RF excitation are shown in Fig. 7b).

L.O.–INDUCED PERFORMANCE LIMITATION

Phase Noise Downconversion

A simplified block diagram of the frequency-locked loop is shown in Figure 8. Here the time dependence of the sensitivity of the measured atomic transition rate is combined with the microwave duty cycle to give an effective time dependent modulation $g(t)$ of the loop gain as shown. In this model, frequency noise $S_y^{LO}(f)$ in the *Local Oscillator* as partially compensated by feedback from the *Integrator* results in *Signal Output* from the locked local oscillator with frequency fluctuations $S_y^{LLO}(f)$. Compensation to achieve high long term stability is accomplished by a feedback circuit in which the *Signal Output* frequency fluctuations are first converted into voltage fluctuations $S_v^d(f)$ by the action of a high Q *Discriminator* and then to $S_v^m(f)$ by the action of the *Modulator*. This voltage is then integrated to provide a correction to the frequency of the *Local Oscillator*.

We identify a loop time constant t_ℓ for the integrator; assuming that for high frequencies $f \gg 1/(2\pi t_\ell)$ the loop gain is approximately zero, while for low frequencies $f \ll 1/(2\pi t_\ell)$ the loop gain is much greater than unity. Thus, high frequency fluctuations will be uncompensated by the action of the loop, so that $S_y^{LLO}(f) = S_y^{LO}(f)$ for $f \gg 1/(2\pi t_\ell)$. However, low frequency fluctuations, as detected, are nearly completely compensated. Thus any down conversion of high frequency components of $S_v^d(f)$ to low frequency components in $S_v^m(f)$ will result in an identical transformation in the locked loop from high frequency components of $S_y^{LO}(f)$ to low frequency components of $S_y^{LLO}(f)$ subject to a requirement of "low" frequency as given above.

Depending on the harmonic content of $g(t)$, the modulator will introduce such down-conversion for "high" frequencies very near integral multiples of $f_c = 1/t_c$ to frequencies near $f = 0$. We assume $t_c \ll t_\ell \ll \tau$, where τ is the time over which the stability of the *Signal Output* is measured. The down-converted signals must be compared to the average value of $g(t)$, the which characterizes the strength with which the modulator passes signals near $f = 0$. For $g(t)$ symmetric about $t = 0$, coefficients g_n for frequency down-conversion of noise amplitudes near the $n$tl harmonic of f_c can be written:

$$g_n = \frac{1}{t_c}\int_0^{t_c} g(t)\cos\left(\frac{2\pi\, n\, t}{t_c}\right) dt, \tag{23}$$

with the average value given by

$$g_0 = \frac{1}{t_c}\int_0^{t_c} g(t)dt. \tag{24}$$

The coefficients g_n depend on the nature of the RF excitation used and can be calculated from forms for $g(t)$ given by Eqs. 10 or 15.

Assuming complete compensation by the loop for the down-converted fluctuations, "white" noise in the narrow range about each harmonic, (and taking into account fluctuations at frequencies both above and below harmonics nf_c,) the low frequency contribution to $S_y^{LLO}(f)$ is given by

$$g_0^2 S_y^{LLO}(0) = 2 \cdot \sum_{n=1}^{\infty} g_n^2 S_y^{LO}(nf_c). \tag{25}$$

The consequences of this relation depend in detail on the nature of the noise which characterizes the

local oscillator and on the time dependence of the duty factor. If, for example, L.O. noise increases rapidly with frequency, the sum may not converge.

Modeling Quartz oscillator performance by a flat Allan Deviation σ_q over the time range of interest allows its flicker frequency noise to be calculated as[13–15]

$$S_y^{LO}(f) = \frac{1}{2\ln(2)} \frac{\sigma_q^2}{f}. \tag{26}$$

Correspondingly, the limiting Ion Standard variance as measured at cycle time t_c can be related to the white noise of the locked loop $S_y^{LLO}(0)$ by

$$\sigma_c^2 = \frac{S_y^{LLO}(0)}{2t_c}. \tag{27}$$

Combining Equations 25–27 allows us to calculate a performance ratio R between the limiting frequency standard performance at the cycle time t_c and the (constant) Quartz oscillator performance given by

$$R^2 \equiv \frac{\sigma_c^2}{\sigma_q^2} = \frac{1}{2\ln(2)} \frac{1}{g_0^2} \sum_{n=1}^{\infty} \frac{g_n^2}{n}. \tag{28}$$

Performance Degradation due to Quartz L.O.

Figure 9 shows the limitations to medium term performance for a trapped mercury ion standard presently under development[5] in terms of the dimensionless parameter R. The effect of conventional feedback limitations due to feedback attack time are also indicated[16,17]. For this L.O. performance[18,19] the value of R would need to be reduced to $R = 0.02$ for this example in order to achieve the stability which is inherent in the standard.

Figure 10 shows the results of numerical calculations of the dependence of R on dead time and pulse time based on Eq. 28 for waveforms shown in Figures 5 and 6. They show that relatively small reduction in R is possible for single pulse RF interrogation, with $R \geq 0.305$ for all values of the dead time. The situation is improved by the use of two (very narrow) pulses where R approaches zero as the dead time is reduced. However, even in that case the requirement of $R \leq 0.02$ to match available quartz L.O.'s to the trapped mercury ion source (from Fig. 9) requires an impractically low dead time of $\Delta_d \approx 0.01$. At present, a minimum value for the trapped mercury ion standard is $\Delta_d \approx 0.1$–0.3.

Cryogenic (superconducting) oscillators[20] are presently available with performance which would match and complement that of the new trapped mercury ion standard. These sources show performance of $\sigma_y(\tau)|_{L.O.} \leq 10^{-14}$ for measuring times 1 second $< \tau <$ 1000 seconds. While they are presently relatively complex and expensive, this may improve; furthermore, if trapped ion performance continues to improve, cryogenic oscillator performance may be required.

The performance improvement made possible by the use of two traps is even greater than may first be apparent. This is because the length of the RF pulse sequence for two traps may be reduced simply by applying more RF power (typically microwatts) and properly synchronizing pulses for the two traps (typically milliseconds). A pulse length of 0.1 second, can be combined with an overall interrogation

time of 10 seconds to give a RF pulse time fraction of $\Delta_{rf} = 0.01$. In contrast, reduction of the dead time much below 1 second in a single trap may prove very difficult on account of the various tasks that must be accomplished during that time. For example, in present versions of the trapped ion standard, a discharge lamp requires approximately 1.0–1.5 seconds for optical interrogation and state preparation during each cycle.

TWO–TRAP CONFIGURATIONS AND SCENARIOS

General Considerations

For two traps in separate and isolated RF environments, Fig. 10 shows that the *optimally overlapping* strategy described in Figs. 6d) and 7a) offers a great advantage, with reduction of L.O. influence on the long–term standard performance by almost 100 times compared to straightforward double–pulse interrogation. *Amplitude modulated* pulses might also be used, for nominally zero effect of the L.O. on medium–term performance.

However, many economies are brought about by combining the vacuum and trapping elements of the two traps. Because trap elements and spacings may be approximately the same size as the wavelength of the exciting radiation, RF isolation between the two traps is likely to be poor. This would require the *100% overlap* strategy described by Fig. 6c), with simultaneous excitation of both traps. As shown in Fig. 10, an RF pulse time of $\Delta_{rf} = 0.01$ would make possible L.O. coupling as low as $R = 0.005$.

Isolated Traps

Figure 11 shows a hardware configuration using two completely independent traps. This design features high RF isolation between traps and great flexibility of operation, so that almost any interrogation scenario could be supported. While this configuration is designed for use with trapped mercury ions in which the RF hyperfine transition at 40.5 GHz is interrogated, similar configurations are applicable to other cases using, e.g. interrogation of optical transitions, state preparation, and/or cooling by the use of lasers at one or more wavelengths. Only those aspects relating to the interrogation process itself are presented: not shown are trapping electrodes and voltage sources, ion sources, etc.

Figure 12 shows a state diagram representing the details of an interrogation scenario using *amplitude modulated* pulses, for the hardware configuration shown in Fig. 11. A similar scenario could be used for any of the other pulse strategies.

Four cycles with length t_c make up this scenario as opposed to two cycles for previously published single trap cases[4–6]. Two cycles are needed for each trap so that a reversal of the RF phase progression can be used to cancel dependence of the frequency on the absolute intensity of signals in the optical system. Thus, for trap #1, the 90° phase advance between RF pulses in cycles 1 and 2 gives rise to a negative dependence of the reading of the counter in cycle 2 (C_2) on the L.O. frequency, while the opposite variation between cycles 3 and 4 gives rise to a corresponding positive dependence of the counter reading in cycle 4.

In this commonly used technique, frequency error is then inferred by the difference between the values of the counts obtained in cycles 2 and 4, or $C_4 - C_2$. Combining the values for the two traps gives an inferred frequency error for the L.O. $\Delta f_{L.O.} \propto C_1 - C_2 - C_3 + C_4$. With appropriate weighting

and filtering, this value is used by the *Control* element of Fig. 11 to adjust the frequency of the *Local Oscillator*, and so compensate and correct its deviations.

Combined Traps in a Linear Structure

Figure 13 shows a configuration that combines two ion collections in linear trapping structure so that a single optical system (lamp and detector) can be used. This configuration is shown in somewhat more detail than the previous one, and the traps share the same RF environment to some extent, so that RF fields must be simultaneously applied to the two traps. Here, electrostatic fields are used to separate and manipulate a linear ion cloud in such a way that its two halves can alternately extend into a central region where optical pumping and detection take place. Electrostatic elements are placed as shown at nodes (zeros) of the RF trapping fields generated by the four circular rods.

Completely overlapping pulses are implemented by the state diagram shown in Fig. 14 with the beginning RF pulse for one trap being one and the same as the ending pulse of the other. Here the phase progression of the RF pulses must extend to 180° in order to provide insensitivity of the frequency to the absolute value of optical signals. This example again gives frequency error in terms of fluorescent light counts in the various cycles as $\Delta f_{L.C.} \propto C_1 - C_2 - C_3 + C_4$.

In the previous configuration, matching values of forward and reverse phase progression ($\pm \approx 90°$) in each trap give a first order cancellation of sensitivity to the actual value of the progression. A similar cancellation here requires that the phase steps at the ends of cycles 1 and 3 match, and also those at the ends of cycles 2 and 4. This could be accomplished by use of two separate 90° phase shifters in series, actuated in an appropriate sequence.

The state diagram for this configuration includes electrostatic potentials for the electrodes which move the ions into and out of the central region for optical illumination. No electrodes are placed in this region because the light they would scatter would degrade performance of the frequency standard. Instead, main electrodes 1 and 4 attract and repel the ions from storage regions at either end where they are subject to RF pulses to begin and end their respective clock cycles. "Cap" electrodes 2 and 3 contain and separate the ion clouds and prevent either ion cloud from mixing with the other. Not shown are electrodes at the trap ends which prevent escape of the ions. Critical aspects of this scenario include stability of the trapping configuration during the clock time "b–e" of either ion cloud as indicated in Fig. 14 while the other cloud is being moved. This is because of a configuration–dependent frequency shift due to second-order Doppler effects[4].

Economies of this configuration include use of one component rather than two for many functions. These components include most of the expensive and performance–sensitive parts of the trap; and include vacuum housing, trap structure, trap excitation electronics, amplitude (pulse) modulator, state pumping lamp and excitation electronics, scattered light detector, and photon counter. The added electrodes complicate the trap structure, but their control with DC potentials is not difficult.

CONCLUSIONS

Improved performance of trapped-ion frequency standards is jeopardized by medium–term instabilities generated by down–conversion of local oscillator frequency fluctuations. These instabilities show a $1/\sqrt{\tau}$ dependence on measuring time τ, and are due to periodic time–variation of the frequency

sensitivity of the RF interrogation process.

We have presented an analysis of the time-variation of this sensitivity for both single- and double-pulse sequential RF interrogation processes based on a spin-flip analogue of the electromagnetic transition process. The consequence of this variation was then numerically calculated for a quartz-crystal type local oscillator with flicker-frequency noise characteristics.

Results of these calculations show that for interrogation processes with large sensitivity variations, e.g. single pulse interrogation with a 50% dead time, the $1/\sqrt{\tau}$ performance of the standard is degraded to a value approximately equal to that of the L.O. when measured at the cycle time for the interrogation process.

Performance can be improved in several ways: (1) Use of an L.O. with ultra-stable short term performance such as the cryogenic SCMO gives a good match to projected Trapped mercury Ion standard performance for almost any interrogation process. (2) Double pulse interrogation with short pulses and with a relatively short dead time (10% or less) can reduce the effect substantially, so that the best Quartz crystal oscillators may not greatly degrade presently observed Trapped Ion performance. (3) Use of several traps with overlapping double-pulse interrogations could greatly reduce, and possibly eliminate, this effect.

Available performance improvement is limited by the inherent stability of the standard, which shows this same time $1/\sqrt{\tau}$ dependence, and by an L.O.-induced "feedback limitation" which decreases more rapidly (as $1/\tau$) with increasing measuring time. Thus the greatest impact on performance takes place at medium and long measuring times ($\tau \geq 1000$ seconds). However, a strength of the trapped ion technology is at these longer times where the great stability achievable with relatively few (isolated) ions can be expressed. Considerations discussed here may also be applicable to future optical trapped ion standards where sequential interrogation is likely to be used, and where L.O. phase noise is also a major concern.

ACKNOWLEDGEMENTS

The authors would like to express their thanks to R. L. Sydnor for his encouragement of this work and to L. S. Cutler for pointing out the problem.

REFERENCES

[1] G. J. Dick, "Calculation of Trapped Ion Local Oscillator Requirements," *Proc. 19th Annual Precise Time and Time Interval (PTTI) Applications and Planning Meeting*, 133-147 (1988).

[2] "A Limit to the Frequency Stability of Passive Frequency Standards," C. Audoin, V. Candelier, and N. Dimarcq, presented at *Conference on Precision Electromagnetic Methods (CPEM)*, Ottawa, Canada, June 11-14, 1990.

[3] F. L. Walls and S. R. Stein "Servo Techniques in Oscillators and Measurement Systems," NBS Technical Note 692, (1976).

[4] J. D. Prestage, G. J. Dick, and L. Maleki, "New Ion Trap for Frequency Standard Applications," *J. Appl. Phys.* 66 (3), 1013-1017, 1989.

[5] J. D. Prestage, G. J. Dick, and L. Maleki, "Linear Ion Trap based Atomic Frequency Standard," *Proc. 44rd Ann. Symp. on Frequency Control*, 82–88 (1990).

[6] L. S. Cutler, R. P. Giffard, P. J. Wheeler, and G. M. R. Winkler, "Initial Operational Experience with a Mercury Ion Storage Frequency Standard," *Proc. 41st Ann. Symp. Freq. Control*, IEEE Cat. No. 87Ch2427–3, 12–19 (1987).

[7] J. Vanier and L. G. Bernier, "On the Signal-to-Noise Ratio and Short-Term Stability of Passive Rubidium Frequency Standards," *IEEE Proc. Instrum. Meas.* IM–30, 277–282 (1981).

[8] J. Vanier and C. Audoin, "Atomic Frequency Standards and Clocks," *J. Phys. E* 9, 697–720 (1976).

[9] J. Vanier and C. Audoin, *The Quantum Mechanics of Atomic Frequency Standards*, Bristol: Adam Hilger, 804 (1989).

[10] D. J. Wineland, J. C. Bergquist, J. J. Bollinger, W. M. Itano, D. J. Heinzen, S. L. Gilbert, C. H. Manney, and C. S. Weimer, "Progress at NIST Toward Absolute Frequency Standards using Stored Ions," it Proc. 43rd Ann. Symp. on Frequency Control, 143–150 (1989).

[11] Kusch, P. and Hughes, V. W., "Atomic and Molecular Beam Spectroscopy," in "Handbuch der Physik," Ed. S. Flügge, Vol. XXXVII/1, p. 55, (1959).

[12] N. F. Ramsey, *Molecular Beams*, London, England, Oxford University Press, (1956).

[13] L. S. Cutler and C. L. Searle, "Some Aspects of the Theory and Measurement of Frequency Fluctuations in Frequency Standards," *Proc. IEEE* 54, 136–154 (1966).

[14] D. W. Allan, "Statistics of Atomic Frequency Standards," *Proc. IEEE* 54, 221–230 (1966).

[15] D. W. Allan, "The Measurement of Frequency and Frequency Stability of Precision Oscillators," *Proc. 6th Ann. Precise Time and Time Interval (PTTI) Applications and Planning Meeting*, 109–142 (1974).

[16] J. Vanier, M. Tetu, and L. G. Bernier, "Transfer of Frequency Stability from an Atomic Frequency Reference to a Quartz-Crystal Oscillator," *IEEE Proc. Instrum. Meas.* IM–28, 188–193 (1979).

[17] A. De Marchi, G. D. Rovera, and A. Premoli, "Effects of Servo Loop Modulation in Atomic Beam Frequency Standards Employing a Ramsey Cavity," *IEEE Trans. Ultrasonics, Ferroelectrics, and Frequency Control* UFFC–34, 582–591 (1987).

[18] Austron BVA Quartz Crystal Oscillator Model 8600, Option 03.

[19] M. B. Bloch, J. C. Ho, C. S. Stone, A. Syed, and F. L. Walls, "Stability of High Quality Quartz Crystal Oscillators: an Update," *Proc. 43rd Ann. Symp. on Frequency Control*, 80–84 (1989).

[20] R. T. Wang and G. J. Dick, "Improved Performance of the Superconducting Cavity Maser at Short Measuring Times," *Proc. 44rd Ann. Symp. on Frequency Control*, 89–93 (1990).

FIGURE CAPTIONS

Figure 1 Field and frequency diagrams for a spin with moment I in the rotating reference system. The general case is shown in a) where the applied frequency ω_{rf} does not match the internal transition frequency $\omega_o = \gamma H_o$, giving rise to an effective field in the rotating frame H_{eff} which differs from the applied RF field H_1. Time evolution of the electromagnetic transition corresponds to a three-dimensional rotation of I about H_{eff}. b) shows evolution during a π pulse at the resonant frequency ω_o.

Figure 2 Three dimensional view of time evolution of I during single-pulse interrogation at a half-bandwidth frequency offset, i.e. final excitation probability is 50%.

Figure 3 Phase variations in the Local Oscillator correspond to rotations about the z axis. Here, an L.O. phase step half-way through the interrogation process causes I_{final} to deviate from the mid-plane (50% excitation probability). L.O. frequency noise can be mathematically represented by a series of such (infinitesimal) phase steps.

Figure 4 Changing the time of the phase step gives differing deviations of the final state from the midplane. Shown are phase steps at 10%, 20%, 40% 60%, 80%, and 90% of the RF pulse time. Phase steps near the middle of the interrogation have a greater effect on excitation probability as represented by the z component of I_{final}.

Figure 5 Time dependence of the sensitivity g(t) of the final state to L.O. frequency variations for several interrogation types. Here, a) corresponds to a sequential appli- cation of single-pulse interrogation as described in detail by Figs. 2, 3, and 4; and b) and c) to double-pulse (Ramsey) interrogation with pulse widths of 20% and 0%, respectively. RF pulses beginning and ending the interrogations are labeled 'b' and 'e'.

Figure 6 Time variability of g(t) may be reduced by the use of alternatively interrogated traps. Here a) shows alternate single-pulse interrogations as Fig. 5a), and b), c), and d) show double-pulse strategies as Fig. 5b) with varying overlap between the beginning pulse for one trap and the ending pulse for the other.

Figure 7 Details of RF pulse sequences for optimally overlapping pulses a) and amplitude-modulated pulses b). Optimally overlapping pulses have a short delay between the ending pulse for one trap and the beginning pulse of the other. Coincident amplitude-modulated pulses with proper waveform give unvarying g(t).

Figure 8 Simplified block diagram of frequency feedback in sequentially interrogated atomic standard. Frequencies near harmonics of t_c^{-1} are aliased to near zero frequency by action of the modulator. High loop gain at long integration times improperly 'corrects' for these perceived low frequency fluctuations.

Figure 9 The effect of aliased (white) low frequency noise can be described in terms of a dimensionless parameter R which describes consequent $1/\sqrt{\tau}$ dependent frequency deviation in relation to L.O. stability and the cycle time t_c. For this example, a value of $R \leq 0.02$ is required to prevent degradation of inherent performance of the source.

Figure 10 Numerical calculations of R for L.O. with flat deviation as shown in Fig. 9 (flicker frequency noise). R is plotted as a function of the fractional dead time Δ_d for one-trap scenarios shown in Figs. 5a) and c); and as a function of fractional RF pulse time Δ_{rf} for two-trap scenarios

described in Figs. 6b), c), and d). Two-trap scenarios show advantage of low-lying curves in addition to ability to reduce $\Delta_{rf} < 0.1$.

Figure 11 Block diagram of a trapped ion frequency standard using two completely independent traps, each including its own phase and amplitude control, state pumping lamp and scattered light detector for maximum flexibility. Excellent RF isolation allows use of complex interrogation scenarios.

Figure 12 State diagram showing a time sequence for the frequency standard as shown above which uses amplitude modulated pulses for nominally zero sensitivity of medium term performance of the standard to L.O. fluctuations. Four cycle scenario allows insensitivity of operating frequency to signal intensity, phase shift error.

Figure 13 Block diagram of a trapped ion frequency standard with two ion collections combined in a single linear quadrupole trapping structure. Added electrostatic electrodes 1–4 separate the ions into two collections and alternately allow each collection to extend into a central region where a state-pumping lamp and scattered light detector are located. Poor RF isolation indicates use of common constant-amplitude RF pulses.

Figure 14 State diagram showing a time sequence for the frequency standard shown above. 180° phase shift range is necessary for insensitivity to signal intensity for both ion collections. Two 90° phase shifters in series can also give independence to phase shift error. V1–V4 show potentials applied to electrostatic electrodes 1–4.

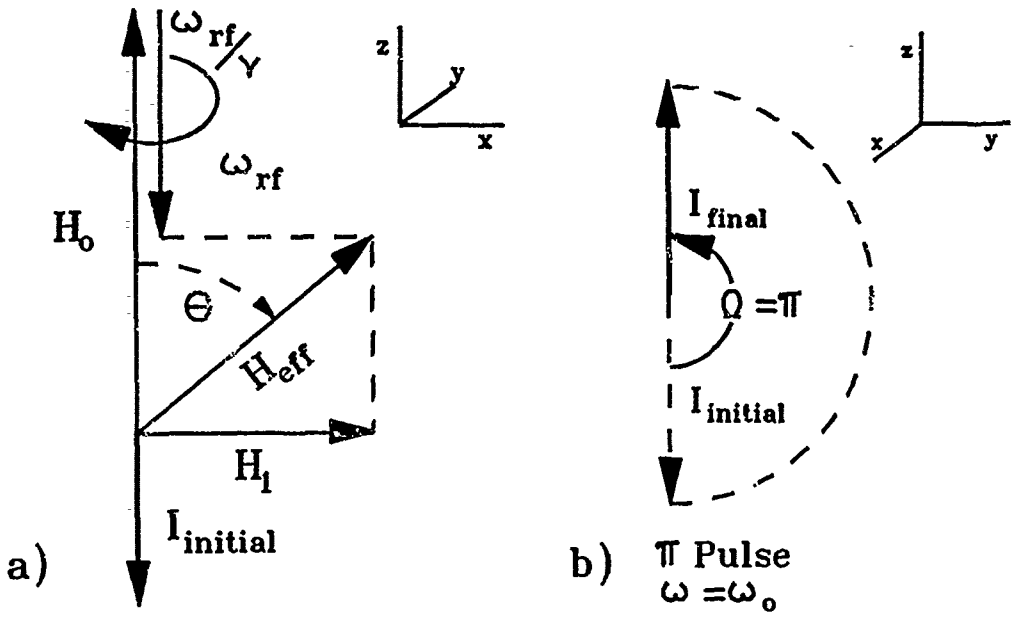

Figure 1: Field and frequency diagrams for a spin with moment I in the rotating reference system. The general case is shown in a) where the applied frequency ω_{rf} does not match the internal transition frequency $\omega_o = \gamma H_o$, giving rise to an effective field in the rotating frame H_{eff} which differs from the applied RF field H_1. Time evolution of the electromagnetic transition corresponds to a three-dimensional rotation of I about H_{eff}. b) shows evolution during a π pulse at the resonant frequency ω_o.

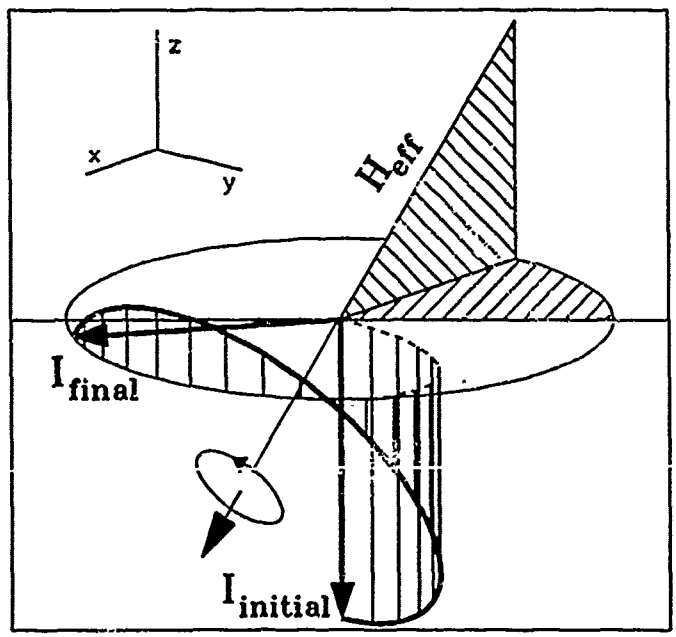

Figure 2: Three dimensional view of time evolution of I during single-pulse interrogation at a half-bandwidth frequency offset, i.e. final excitation probability is 50%.

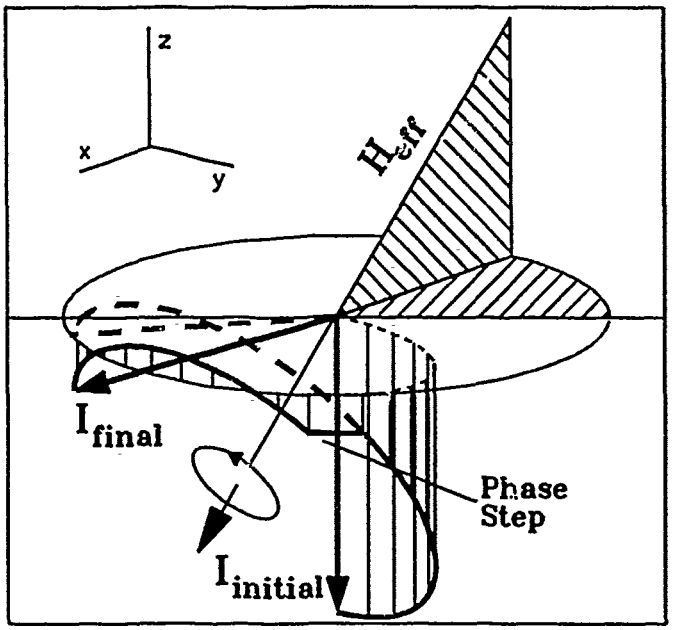

Figure 3: Phase variations in the Local Oscillator correspond to rotations about the **z** axis. Here, an L.O. phase step half-way through the interrogation process causes I_{final} to deviate from the mid-plane (50% excitation probability). L.O. frequency noise can be mathematically represented by a series of such (infinitesimal) phase steps.

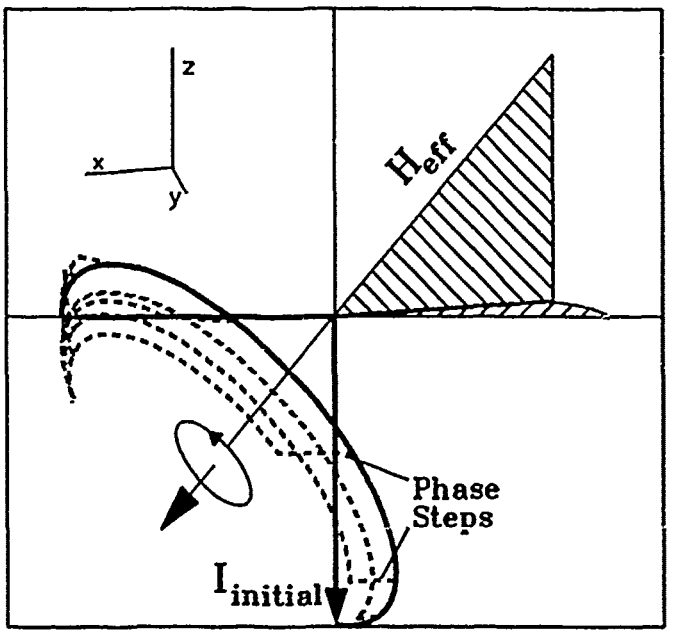

Figure 4: Changing the time of the phase step gives differing deviations of the final state from the midplane. Shown are phase steps at 10%, 20%, 40% 60%, 80%, and 90% of the RF pulse time. Phase steps near the middle of the interrogation have a greater effect on excitation probability as represented by the z component of I_{final}.

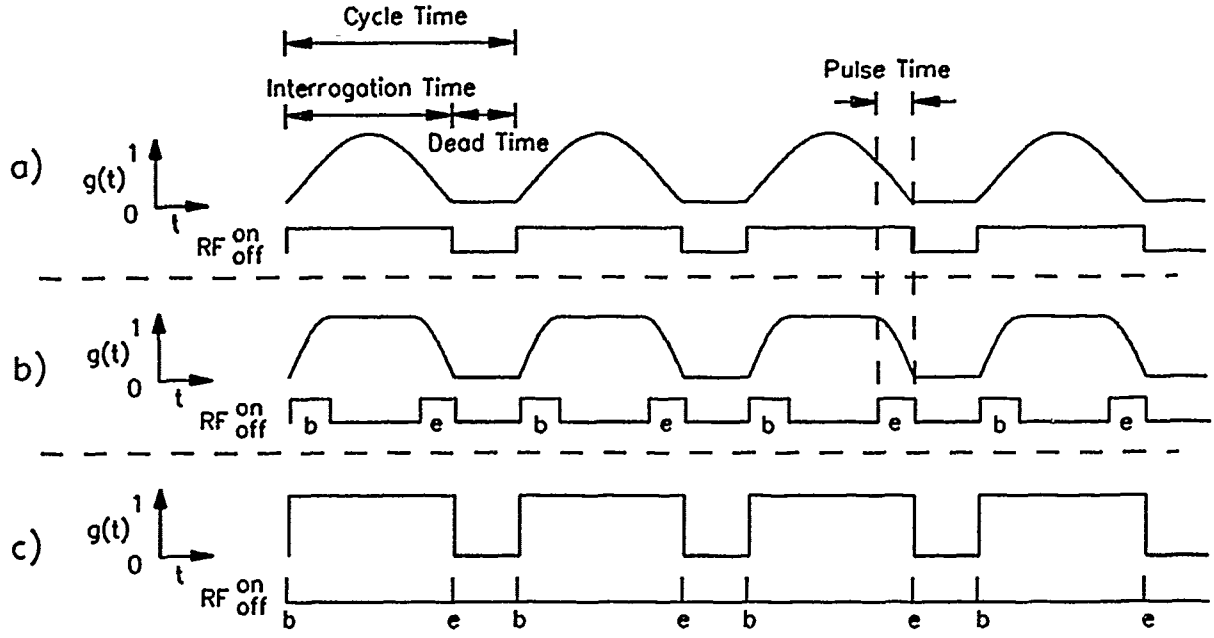

Figure 5: Time dependence of the sensitivity g(t) of the final state to L.O. frequency variations for several interrogation types. Here, a) corresponds to a sequential application of single-pulse interrogation as described in detail by Figs. 2, 3, and 4; and b) and c) to double-pulse (Ramsey) interrogation with pulse widths of 20% and 0%, respectively. RF pulses beginning and ending the interrogations are labeled 'b' and 'e'.

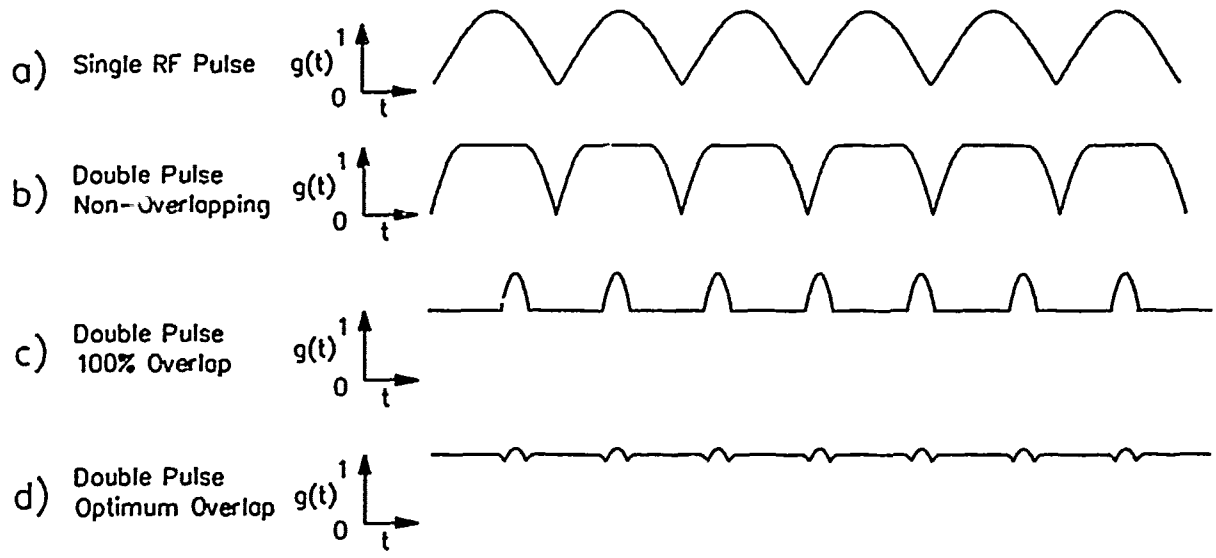

Figure 6: Time variability of g(t) may be reduced by the use of alternatively interrogated traps. Here a) shows alternate single-pulse interrogations as Fig. 5a); and b), c), and d) show double-pulse strategies as Fig. 5b) with varying overlap between the beginning pulse for one trap and the ending pulse for the other.

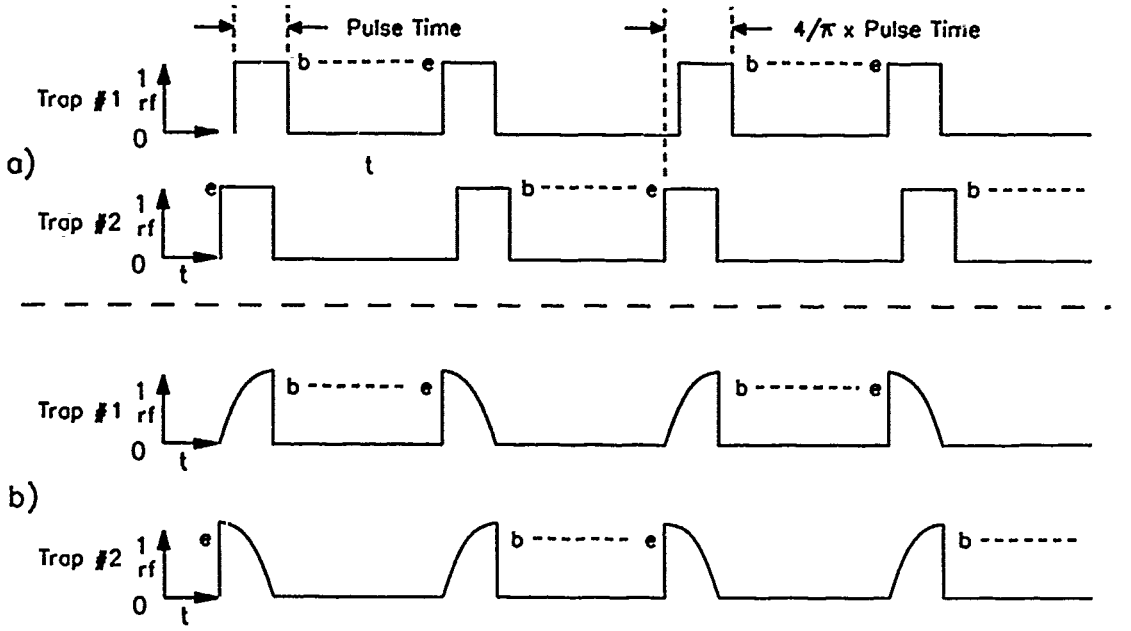

Figure 7: Details of RF pulse sequences for optimally overlapping pulses a) and amplitude-modulated pulses b). Optimally overlapping pulses have a short delay between the ending pulse for one trap and the beginning pulse of the other. Coincident amplitude-modulated pulses with proper waveform give unvarying g(t).

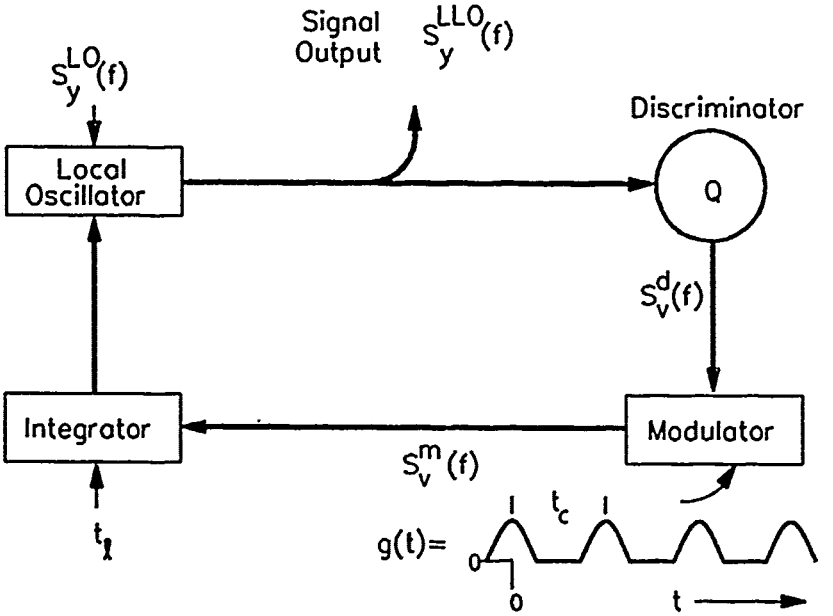

Figure 8: Simplified block diagram of frequency feedback in sequentially interrogated atomic standard. Frequencies near harmonics of t_c^{-1} are aliased to near zero frequency by action of the modulator. High loop gain at long integration times improperly 'corrects' for these perceived low frequency fluctuations.

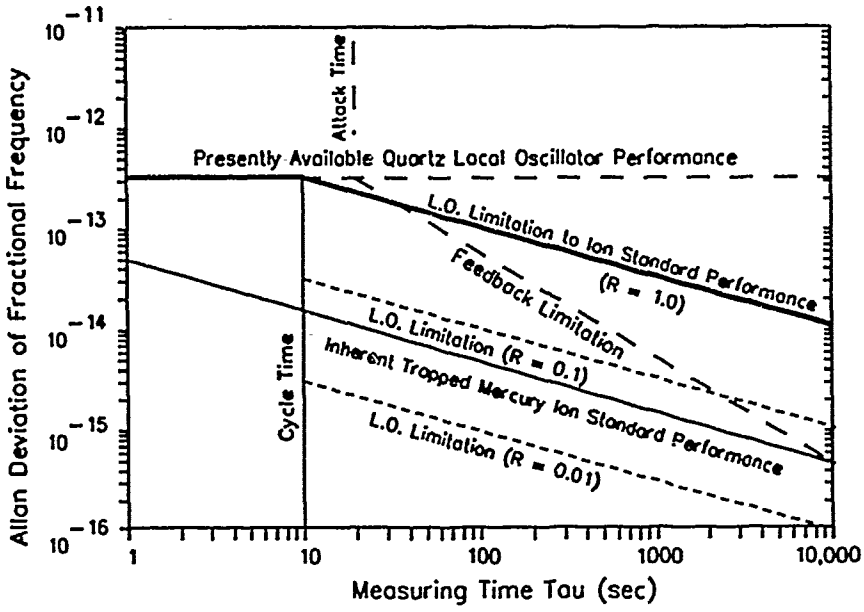

Figure 9: The effect of aliased (white) low frequency noise can be described in terms of a dimensionless parameter **R** which describes consequent $1/\sqrt{\tau}$ dependent frequency deviation in relation to L.O. stability and the cycle time t_c. For this example, a value of $\mathbf{R} \leq 0.02$ is required to prevent degradation of inherent performance of the source.

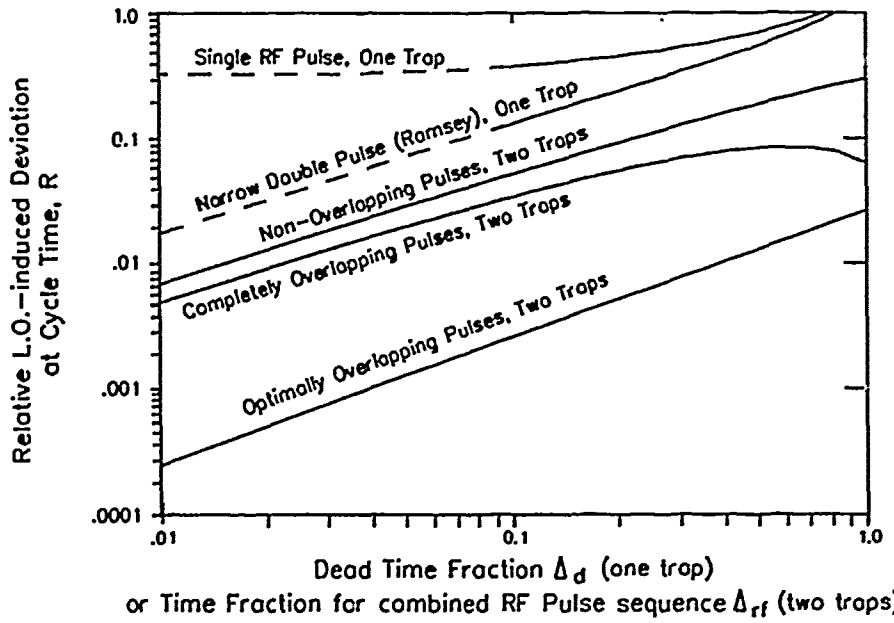

Figure 10: Numerical calculations of **R** for L.O. with flat deviation as shown in Fig. 9 (flicker frequency noise). **R** is plotted as a function of the fractional dead time Δ_d for one-trap scenarios shown in Figs. 5a) and c); and as a function of fractional RF pulse time Δ_{rf} for two-trap scenarios described in Figs. 6b), c), and d). Two-trap scenarios show advantage of low-lying curves in addition to ability to reduce $\Delta_{rf} < 0.1$.

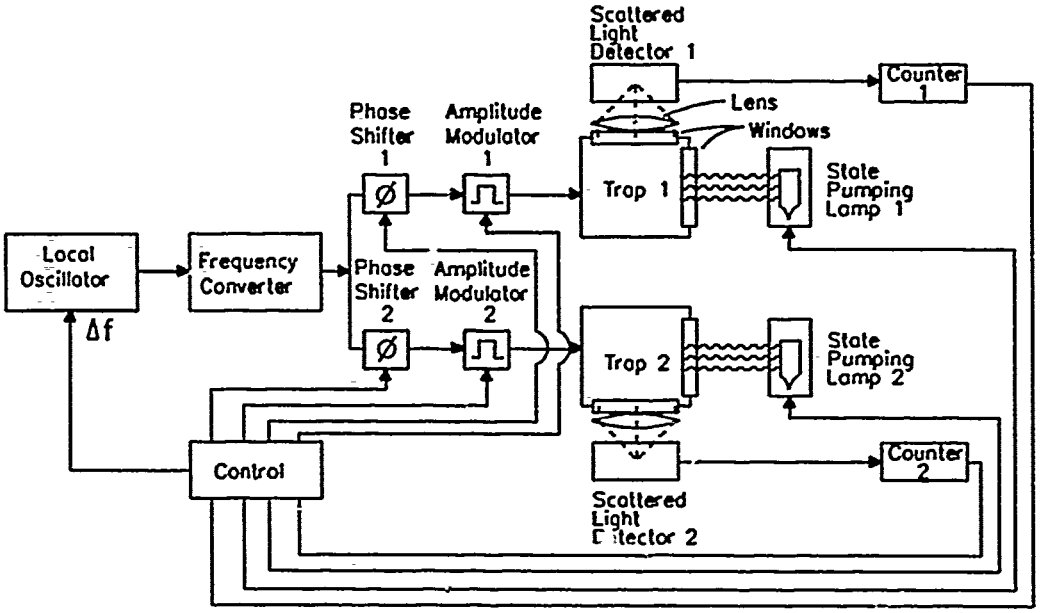

Figure 11: Block diagram of a trapped ion frequency standard using two completely independent traps, each including its own phase and amplitude control, state pumping lamp and scattered light detector for maximum flexibility. Excellent RF ... lation allows use of complex interrogation scenarios.

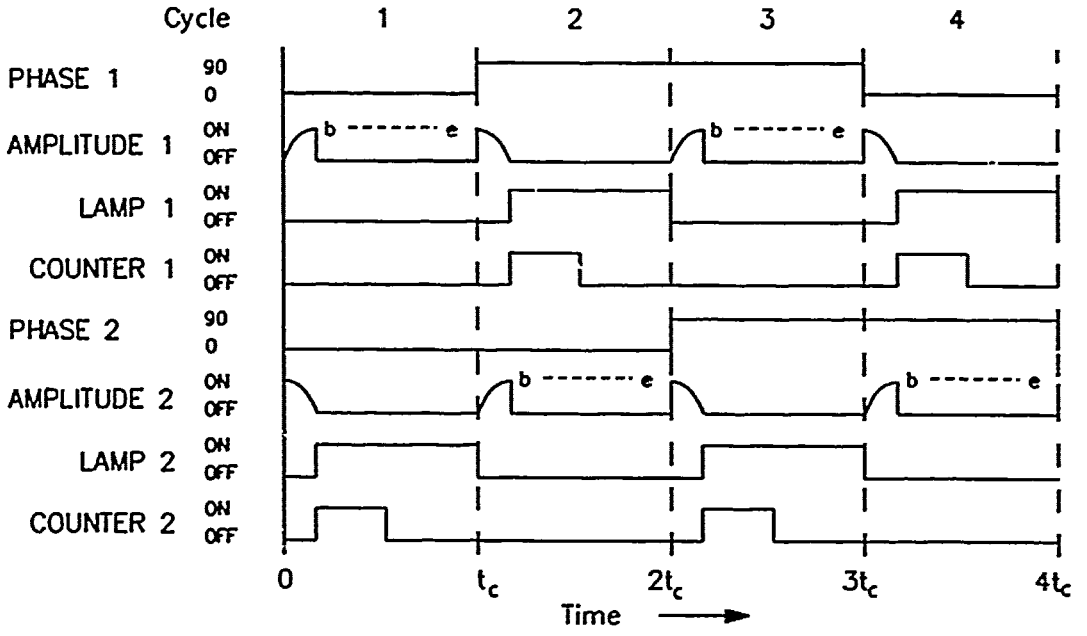

Figure 12: State diagram showing a time sequence for the frequency standard as shown above which uses amplitude modulated pulses for nominally zero sensitivity of medium term performance of the standard to L.O. fluctuations. Four cycle scenario allows insensitivity of operating frequency to signal intensity, phase shift error.

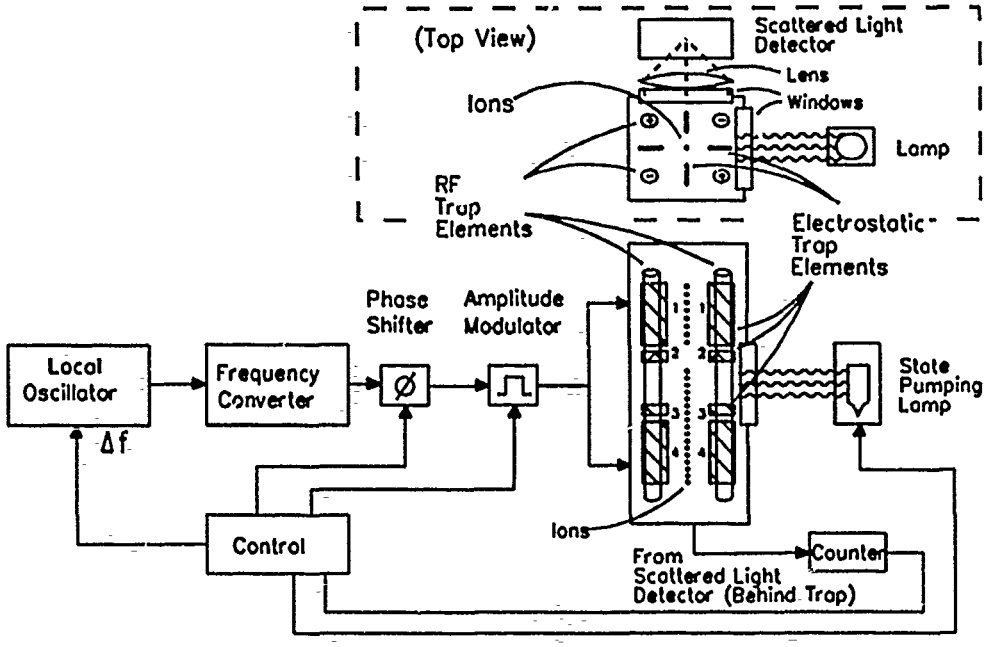

Figure 13: Block diagram of a trapped ion frequency standard with two ion collections combined in a single linear quadrupole trapping structure. Added electrostatic elements 1-4 separate the ions into two collections and alternately allow each collection to extend into a central region where a state-pumping lamp and scattered light detector are located. Poor RF isolation indicates use of common constant-amplitude RF pulses.

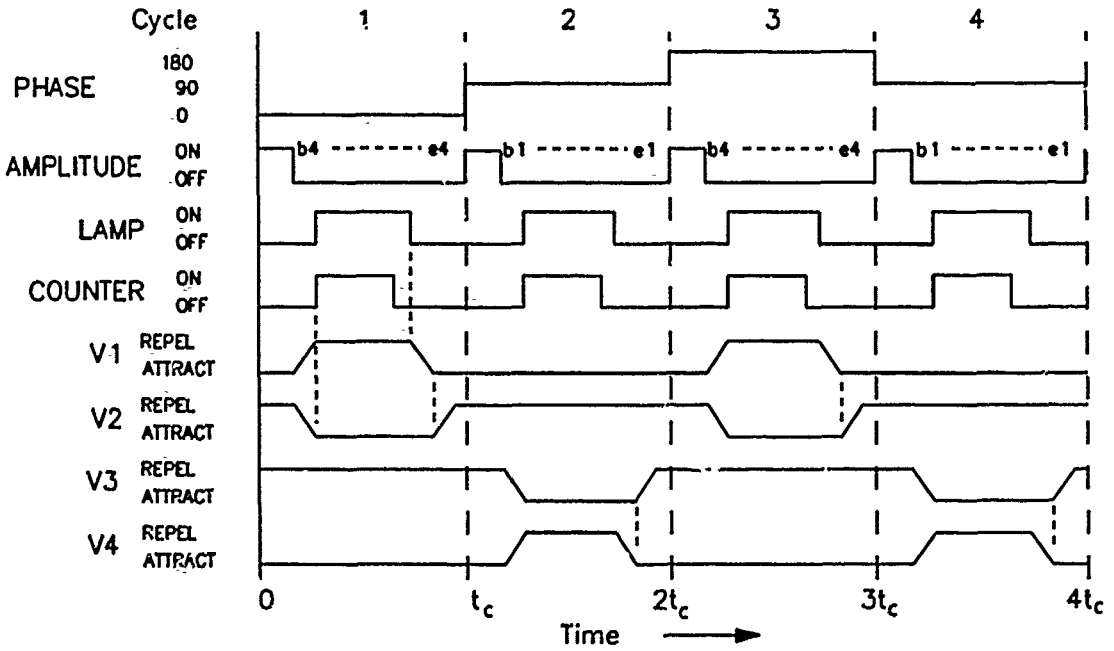

Figure 14: State diagram showing a time sequence for the frequency standard shown above. 180° phase shift range is necessary for insensitivity to signal intensity for both ion collections. Two 90° phase shifters in series can also give independence to phase shift error. V1-V4 show potentials applied to electrostatic electrodes 1-4.

PERFORMANCE OF SOVIET AND U.S. HYDROGEN MASERS

Adolf A. Uljanov and Nikolai A. Demidov
"Quartz" Research and Production Association, Gorkii, USSR

Edward M. Mattison and Robert F. C. Vessot
Smithsonian Astrophysical Observatory, Cambridge, Massachusetts, USA

David W. Allan
National Institute of Standards and Technology, Boulder, Colorado, USA

Gernot M. R. Winkler
United States Naval Observatory, Washington, D.C., USA

ABSTRACT

The frequencies of Soviet- and U.S.-built hydrogen masers located at the Smithsonian Astrophysical Observatory and at the United States Naval Observatory (USNO) were compared with each other and, via GPS common-view measurements, with three primary frequency-reference scales. The best masers were found to have fractional frequency stabilities as low as 6×10^{-16} for averaging times of approximately 10^4 s. Members of the USNO maser ensemble provided frequency prediction better than 1×10^{-14} for periods up to a few weeks. The frequency residuals of these masers, after removal of frequency drift and rate of change of drift, had stabilities of a few parts in 10^{-15}, with several masers achieving residual stabilities well below 1×10^{-15} for intervals from 10^5 s to 2×10^6 s. The fractional frequency drifts of the 13 masers studied, relative to the primary reference standards, ranged from -0.2×10^{-15}/day to $+9.6\times10^{-15}$/day.

INTRODUCTION

A welcome consequence of *glasnost*, the Soviet movement to openness, has been the recent availability of Soviet-built hydrogen masers for testing in the United States. In September 1990, two atomic hydrogen masers built by the Gorkii Instrument-Making Research and Development Institute were shipped to the Smithsonian Astrophysical Observatory (SAO) for comparison with U.S.-built masers and with time scales throughout the world. This unprecedented event was a result of discussions among officials of the U.S. National Institute of Standards and Technology (NIST), the Soviet "Quartz" Research and Production Association, and SAO.

Because of the previous scarcity of information on Soviet masers, the initial and primary interest of the comparisons was on the performance of the Soviet masers; however, for two reasons the scope of the work expanded to include other frequency standards. First, the frequency of a clock cannot be evaluated in isolation, but must be measured relative to accepted primary references; thus it was important to compare the masers at SAO with international time scales. Second, the use of common-view Global Positioning System (GPS) comparisons made it possible to include in the study an ensemble of nine hydrogen masers located at the United States Naval Observatory (USNO). In addi-

tion to being used to extend the TAI time scale over the period of observation, these masers represent a cohort of state-of-the art frequency standards whose performance has not previously been reported on. Thus we have evaluated a substantial number of hydrogen masers produced by manufacturers worldwide.

MASERS STUDIED

Four of the masers under study were located at the SAO Maser Laboratory. Two of these, serial numbers P13 and P26, are model VLG-11 masers built by the SAO Maser Group. The Soviet masers[1,2] at SAO were a model Ch1-75 active maser and a model Ch1-76 passive maser[3]. All masers other than Ch1-76 were active oscillators. Maser Ch1-75 is equipped with an autotuning system designed to stabilize the resonance frequency of the maser's microwave cavity, and thus reduce frequency variations due to cavity pulling. The autotuner, which was operated during part of this study employs linewidth modulation by means of alternation of the internal magnetic field gradient at intervals of 100 s; a high-stability signal from another maser is used as a reference for the system. Masers P13 and P26 do not use cavity autotuners.

Nine masers at the USNO were studied. Three were SAO VLG-11 masers, serial numbers P18, P19, and P22; two were SAO VLG-12 masers[4], numbers P24 and P25; and four were commercial masers[5], serial numbers N2, N3, N4, and N5.

The masers were compared with each other and with three primary time scales, TAI, NIST(AT1), and UTC(PTB). TAI (International Atomic Time) is maintained by the Bureau International des Poids et Mesures (BIPM) in Sevres, France; it incorporates time and frequency data from about 180 clocks located in more than 50 standards laboratories throughout the world. NIST(AT1) is an unsteered, unsyntonized cesium-generated time scale maintained by the NIST Time and Frequency Division, Boulder, Colorado. Its generating algorithm, AT1, is optimized for frequency stability and minimum time prediction error. UTC(PTB), generated at the Physikalische-Technische Bundesanstalt in Braunschweig, Germany, is controlled by PTB primary cesium standard Cs-1.

TIME AND FREQUENCY COMPARISON SYSTEMS

Several time and frequency comparison systems were employed to link the masers and the time scales, and to provide measurements of frequency stability over both short and long time spans.

Three systems were used at SAO to compare the masers located there (Fig. 1). Frequency difference measurements for intervals of 0.8 s and longer were made with SAO's beat-frequency measurement facility, which permits two or three masers to be compared simultaneously. The masers' frequency synthesizers are offset from one another, and their receiver output signals are multiplied to 1.2 GHz and mixed in highly isolated double-balanced mixers. The periods of the resulting beat signals are measured by a three-channel, zero-deadtime counter and stored in a computer. Typically the frequency synthesizers are offset from one another by approximately 1.4 Hz at 1.42 GHz; after division to the 1.2 GHz comparison frequency, the beat frequency is approximately 1.18 Hz, corresponding to a beat period of approximately 0.84 s. When three masers are compared using